Mg^{2+} binding to Coenzyme A

Jonathan A. Semelak[1,2 *], Mariana Gallo[3], F. Luis González Flecha[4], Solana Di Pino[1,2], Thelma A. Pertinhez[3], Ari Zeida[5,6], Ivan Gout[7,8], Dario A. Estrin[1,2], Madia Trujillo[5,6 *]

1- CONICET-Universidad de Buenos Aires, Instituto de Química Física de los Materiales, Medio Ambiente y Energía (INQUIMAE), Buenos Aires, Argentina.
2- Universidad de Buenos Aires, Facultad de Ciencias Exactas y Naturales, Departamento de Química Inorgánica, Analítica y Química Física, Buenos Aires, Argentina.
3- Laboratory of biochemistry and Metabolomics, Department of Medicine and Surgery, University of Parma, Italy.
4- Laboratorio de Biofísica Molecular, Instituto de Química y Fisicoquímica Biológicas, Universidad de Buenos Aires, CONICET, Buenos Aires, Argentina.
5- Departamento de Bioquímica, Facultad de Medicina, Universidad de la República, Montevideo 11800, Uruguay.
6- Centro de Investigaciones Biomédicas (CEINBIO), Universidad de la República, Montevideo 11800, Uruguay.
7-Department of Structural and Molecular Biology, University College London, London WC1E 6BT, UK.
8- Institute of Molecular Biology and Genetics, National Academy of Sciences of Ukraine, 03680 Kyiv, Ukraine.

[*] Corresponding authors: Jonathan A. Semelak, e-mail jsemelak@qi.fcen.uba.ar and Madia Trujillo, e-mail madiat@fmed.edu.uy

Highlights

- Mg^{2+} binds to CoA in a 1:1 ratio with K_a of 537 M^{-1} (pH 7.2) and 312 M^{-1} (pH 7.8).
- Both in cytosol and mitochondria the fraction of CoA as CoA-Mg^{2+} would be significant.
- The binding is entropically driven, and the associated entropic gain seems solvent-related.
- The coordination occurs mainly through the diphosphate group.
- The conformational landscape of CoA is severely modified upon Mg^{2+} binding.

Abstract

Magnesium (Mg^{2+}), the second most abundant intracellular cation, plays a crucial role in cellular functions. In this study, we investigate the interaction between Mg^{2+} and coenzyme A (CoA), a thiol-containing cofactor central to cellular metabolism also involved in protein modifications. Isothermal titration calorimetry revealed a 1:1 binding stoichiometry between Mg^{2+} and free CoA under biologically relevant conditions. Association constants of (537 ± 20) M^{-1} and (312 ± 7) M^{-1} were determined at 25°C and pH 7.2 and 7.8, respectively, suggesting that a significant fraction of CoA is likely bound to Mg^{2+} both in the cytosol and in the mitochondrial matrix. Additionally, the process is entropically-driven, and our results support that the origin of the entropy gain is solvent-related. On the other hand, the combination of 1- and 2-dimensional nuclear magnetic resonance spectroscopy with molecular dynamics simulations and unsupervised learning demonstrate a direct coordination between Mg^{2+} and the phosphate groups of the 4-phosphopantothenate unit and bound to position 5' of the adenosine ring. Interestingly, the phosphate in position 3' only indirectly contributes to Mg^{2+} coordination. Finally, we discuss how the binding of Mg^{2+} to CoA perturbates the chemical environment of different CoA atoms, regardless of their apparent proximity to the coordination site, through the modulation of the CoA conformational landscape. This insight holds implications for understanding the impact on both CoA and Mg^{2+} functions in physiological and pathological processes.

Keywords: Coenzyme A, magnesium, mitochondria, NMR, calorimetry, molecular dynamics

Introduction

Magnesium is the second most abundant intracellular cation after potassium. In biological systems it exists typically as Mg^{2+}. Its concentration in cells is high, in the order of 10-30 mM, and it is mostly bound to organic compounds such as ATP, phospholipids, proteins and nucleic acids.[1,2] The concentration of free Mg^{2+} in cells has been estimated as 0.5-1.2 mM.[3,4] It is a cofactor for more than 600 enzymes and a regulator of ion channels, thus being essential for various cellular functions.[2,5] At least one-third of total magnesium is in the mitochondria, where it is concentrated due to the actions of Msr2, a selective transporter found in the inner mitochondrial membrane.[6] Magnesium regulates mitochondrial transmembrane potential, bioenergetics, and redox state, suggesting that this metal should be considered an essential element for mitochondrial function in mammalian cells.[7]

Coenzyme A (CoA) is a thiol-containing cofactor that plays key roles in many life processes.[8–10] It is present in all living organisms, both free and as thioester derivatives such as acetyl and acyl CoA, and plays essential roles in cellular functions as varied as metabolism, gene expression, and cell death.[11] The discovery of CoA and the determination of its structure led to Fritz Albert Lipmann being awarded the Nobel Prize in Physiology or Medicine in 1953.[12] CoA is composed of a 4-phosphopantothenate unit bound by a phosphoric anhydride linkage to an adenosine 3',5'-diphosphate unit and by an amide bond to cysteamine (Figure 1).

CoA and its derivatives promote different protein post-translational modifications, which can affect protein structure, distribution and function, including protein acetylation and acylation,[13,14] 4'-phosphopantetheinylation and formation of mixed disulfides with Cys residues in a process that is referred to as protein CoAlation.[15–17] In mammals, the concentration of CoA and its derivatives varies in different tissues, being highest in the liver and cardiac muscle.[18] Furthermore, CoA and its derivatives are compartmentalized inside the cell: levels of CoA in mitochondria are in the mM range (2.55-3.35 mM in the case of non-acylated CoA), while in peroxisomes, cytosol, nucleus, and endoplasmic reticulum it is present at lower concentrations.[19] In fact, specific CoA and dephosphoCoA transporters were detected in mitochondrial and peroxisome membranes.[20]

CoA presents multiple potential metal binding sites, including the cysteamine and the 3',5'-adenosine diphosphate portions. Indeed, Ni^{2+} was reported to coordinate with the sulfur at cysteamine and Co^{2+} to bind to the adenosine unit[21] of the cofactor.[22] Other ions that interact with CoA are Hg^{2+} and Mn^{2+}.[23,24] The fact that Mg^{2+} can bind to different phosphate- and, with greater affinity, pyrophosphate-containing moieties such as ATP, UTP, ADP, UDP, thiamine pyrophosphate and free pyrophosphate, suggests that it could also bind CoA.[22,25–28] Indeed, Mg^{2+} reduced the inhibition of several enzymes by pyrophosphate-containing compounds, including CoA, suggesting that the cation could compete with the enzymes for the compounds.[29] Furthermore, the crystal structure of several CoA-dependent proteins shows that Mg^{2+} is frequently present in ternary complexes consisting in protein, CoA and Mg^{2+} (sometimes the latter is substituted by Mn^{2+}).[30,31] However, structural and

thermodynamic data regarding the interaction between free CoA and Mg^{2+} is lacking so far, precluding the estimation of the percentage of CoA that would be bound to the metal in the different cell compartments. Herein we measured the association constant of Mg^{2+} for free CoA under different biologically relevant conditions, studied the binding mode of the complex through NMR spectroscopy, and complemented the experiments with computer simulations. Our data indicate that at least in the mitochondrial matrix, where the concentrations of CoA and Mg^{2+} are relatively high, an important fraction of the cofactor is expected to be bound to Mg^{2+} which could affect both CoA and Mg^{2+} functions in physiopathological processes.

Experimental and Computational Methods

Reagents and Materials

The trilithium salt of CoA, $MgCl_2$ anhydrous, Trizma pre-set crystals (pH 7.2), Chelex 100 sodium form, and trimethylsilyl propanoic acid (TSP) were purchased from Sigma Aldrich. Deuterium oxide (D_2O) was obtained from Cambridge Isotope Laboratories, Inc.

Isothermal Titration Calorimetry (ITC) Analysis

Thermodynamic characterization of the interaction between Mg^{2+} and CoA was performed by ITC using a Microcal VP-ITC microcalorimeter. CoA solutions were freshly prepared in a buffer whose composition is indicated in the legend for Figure 2, and their concentrations were determined by registering the absorption spectra between 230 and 340 nm, using a molar absorption coefficient of 14,328 M^{-1} cm^{-1} at 258 nm.[32] Thiol content in CoA solutions was measured at 412 nm by the Ellman's assay[33], and confirmed that it was more than 90% reduced. Furthermore, incubations of CoA (1.5 mM) for 3 hours in degassed Tris/Cl buffer 100 mM pH 7.8 and 25°C used in ITC experiments caused less than 5% thiol oxidation, consistently with the previously reported low autoxidation rate of CoA compared with those of glutathione and cysteine.[34] The concentrations of Mg^{2+} solutions were determined by titration against ethylenediamine tetraacetic acid (EDTA).[35] In a typical experiment, CoA was loaded into the sample cell and $MgCl_2$ in the injector, and after an initial 60 s equilibration, the experiments started with a first injection of 2 µL and successive injections every 200 s with the syringe stirring speed set at 286 rpm. Heats of dilution of $MgCl_2$ in the corresponding buffer were determined in parallel experiments where CoA was replaced by only buffer in the sample cell, and were subtracted from each data set.

The following equation accounts for the relationship between the integrated heat (normalized by mol of $MgCl_2$ injected, (Q_i)) and the binding density at the injection i ($\langle n_i \rangle$).

$$Q_i = V_c \langle n \rangle_i [CoA]_o \Delta H \quad (1)$$

Where, $[CoA]_o$ is the initial concentration of CoA in the cell, ΔH is the molar association enthalpy and V_c the cell volume. This equation was used for global fitting to each set of experiments performed with several initial CoA concentrations, using a nonlinear regression procedure.[36] Different binding models were assayed,[37] and the best fit to the experimental data was obtained with a model of identical and independent binding sites:

$$\langle n \rangle = \frac{1}{2}\left\{\left(\frac{1}{k \cdot [CoA]_T} + \frac{[Mg^{2+}]_T}{[CoA]_T} + N\right) - \sqrt{\left(\frac{1}{k \cdot [CoA]_T} + \frac{[Mg^{2+}]_T}{[CoA]_T} + N\right)^2 + 4N\frac{[Mg^{2+}]_T}{[CoA]_T}}\right\} \quad (2)$$

Where N is the binding stoichiometry, k is the microscopic association constant, and $[Mg^{2+}]_T$ and $[CoA]_T$ are the total (free + bound) concentrations at the injection *i*. The Gibbs free energy change for association in the reference state (ΔG^0_a) and the entropic contribution to ΔG^0_a were calculated following the classical equilibrium thermodynamic relationships.

NMR spectroscopy

NMR experiments were performed at the CIM - Centro Interdipartimentale Misure "Giuseppe Casnati", University of Parma. A 3.5 mM CoA solution in 50 mM Tris buffer pH 7.2 containing 5% D_2O and 1 mM TSP was initially prepared and used as an internal standard for CoA quantification. Magnesium displacement experiments were conducted by adding 2.5 M $MgCl_2$ in the same buffer to the CoA solution to final magnesium concentrations of 200, 350, and 500 mM. The subsequent solutions were prepared in a 50 mM Tris buffer in D_2O and previously treated with Chelex 100 to remove possible divalent metal cation traces. All the CoA solutions were freshly prepared, and their pH was adjusted to 7.2.

To investigate chemical shift perturbations of CoA upon interaction with Mg^{2+}, a 5 mM CoA solution at pH 7.2 was prepared and 2.5 M $MgCl_2$ in D_2O was added to final magnesium concentrations of 50 and 150 mM. The pH of the final solution was checked to remain invariable. For the combined carbon-proton chemical shift perturbations, we used the following equation:

$$\Delta\delta_{^1H-^{13}C} = \sqrt{\frac{\Delta\delta^2_{^1H} - \alpha\Delta\delta^2_{^{13}C})}{2}} \quad (3)$$

where α = 0.06, as evaluated considering the ratio for observed hydrogen and carbon chemical shift ranges for CoA (8.00 and 140.0 ppm, respectively).[38]

NMR experiments were performed at 25°C using a Bruker Avance 400 spectrometer equipped with a 5 mm Prodigy cryoprobe. One-dimensional ^{1}H and ^{31}P NMR hydrogen decoupled spectra were recorded on all the samples, while 2D ^{1}H-^{13}C HSQC spectra were also acquired on 5 mM CoA samples without and with 50 or 150 mM $MgCl_2$. The CoA titration with $MgCl_2$ was monitored using 1D ^{1}H and ^{31}P and 2D ^{1}H-^{13}C spectra. For the ^{1}H experiments, standard 1D NOESY spectra with presaturation for single solvent suppression (noesypr1d pulse sequence) were acquired. Thus, the residual water signal in the D_2O solutions was suppressed. Spectral width was 6400 Hz; 5 to 10 s, the recycle delay; and 32 transients were recorded with 32768 time domain data points. In the ^{31}P spectra, 1D sequences with ^{1}H powered-gated decoupling and using a 30-degree flip angle (zg30 pulse program) were used with a spectral width of 12931 Hz, 2 s of recycle delay, 32 transients, and 131072 time domain data points. The ^{1}H-^{13}C HSQC spectra used an HSQC sequence with Echo/Antiecho-TPPI (time proportional phase incrementation) acquisition mode in F1, sensitivity improvement, and gradient and shaped (selective) pulses (hsqcetgpsisp2.2 pulse sequence[39]). The spectra had a spectral width of 5198 Hz and 17123 Hz for the ^{1}H and ^{13}C dimensions, 512 t1 increments, each with 2048 complex data points, 4 transients, and a relaxation delay of 2.0 s. NMR data acquisition, processing, and analyses was performed using the Bruker software package TopSpin. The CoA atom numbering system used in this paper is indicated in **Figure 1**.

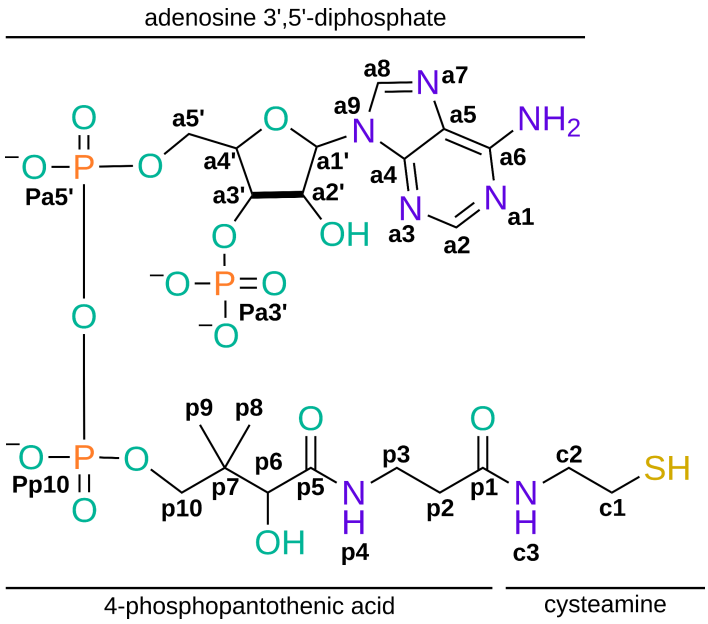

Figure 1. Coenzyme A chemical structure and atom numbering system used in this study. Atoms are labeled according to their positions in the corresponding fragments: **ci** for position **i** in the cysteamine fragment, **pi** for position **i** in the 4-phosphopantothenic acid fragment, and **ai** for position **i** in the

adenine ring and **ai'** for position **i** in the ribose ring; additionally, phosphorus atoms are labeled starting with a capital **P**. In order to facilitate the NMR assignment, we used a numbering scheme that closely resembles the one proposed by Dordine et. al.[40]

By monitoring the chemical shifts of the most perturbed nuclei (hydrogens **a8**, **a5'B**, and **a3'** and phosphorus **Pp10'**) for 1:10 and 1:30 equivalent ratios of CoA:Mg^{2+}, at 5 mM CoA concentration, the K_a value was estimated, considering a 1:1 stoichiometry, according to the following equation[38]:

$$\frac{\Delta\delta_{\mathrm{obs}}}{\Delta\delta_{\mathrm{obs,max}}} = \frac{\mathrm{a} - \sqrt{\mathrm{a}^2 - 4[\mathrm{CoA}]_{\mathrm{T}}[\mathrm{Mg}^{2+}]_{\mathrm{T}}}}{2[\mathrm{CoA}]_{\mathrm{T}}} \qquad (4)$$

Where, $\Delta\delta_{obs}$ is the chemical shift perturbation observed, $\Delta\delta_{obs,max}$ is the chemical shift perturbation observed at the highest magnesium concentration (150 mM), and $a = [CoA]_T + [Mg^{2+}]_T + K_a^{-1}$. Note that equation (2) equals equation (4) if we consider $\langle n\rangle = \Delta\delta_{obs}/\Delta\delta_{obs,max}$, N = 1 and $k = K_a$.

Molecular dynamics simulations setup and general procedures

Classical molecular dynamics (MD) simulations were carried out to characterize the conformational changes in the CoA molecule induced by the coordination of Mg^{2+}, and its associated entropy change. The simulations consisted of a single CoA molecule in aqueous solution, both in absence and presence of a single Mg^{2+} ion coordinated through the phosphate groups, following previous ITC studies[26,27] of Mg^{2+} binding to ATP, and the experimental results obtained herein. The MD simulations were carried out with the AMBER16 package.[41] Parameters for the CoA molecule with the thiol in its protonated form were obtained from the Generalized Amber Force Field (GAFF)[42] using Antechamber and Parmcheck, employing restrained electrostatic potential (RESP)[43] charges fitted from the electron density obtained at the Hartree-Fock/6-31G* level of theory *in vacuo*, using Gaussian09[44] Mg^{2+} ion parameters correspond to the ions94 forcefield.[45,46] A single CoA molecule was solvated with about 11500 TIP3P water molecules in a truncated octahedral box, using Leap, from the AMBER16 package.[41] The MD simulations were carried out with periodic boundary conditions with a 10 Å cutoff and the SHAKE algorithm to keep hydrogen bond lengths at their equilibrium distance.[47] The system was heated to 27°C gradually, with the Berendsen thermostat.[48] Then, the density was adjusted in 0.5 ns in the NPT ensemble (constant amount of substance, pressure and temperature) with the Berendsen barostat and thermostat (1 bar and 27°C).[48] Next, 100 ns of MD were simulated in the NVT ensemble (similar to NPT but with constant volume instead of pressure), using a time step of 2 fs, and the Langevin thermostat to keep the temperature around 27°C.[49] 5 frames were extracted from the obtained trajectory, and 500 ns long MD were simulated starting from each of these frames. The 5 trajectories summed a total sampling time of 2.5 μs, both for CoA and the CoA-Mg^{2+} complex.

Configurational entropy estimation

The molar configurational entropy (S_{conf}) was estimated from the mass-weighted covariance matrix using the Schlitter's method[50], which has been applied to a broad spectrum of biomolecular systems[51,52] and establishes that the absolute molar configurational entropy can be estimated from a MD trajectory of length *t* as:

$$\mathrm{S_{conf}(t)} = \frac{\mathrm{R}}{2} \ln det \left\{ \mathbf{1} + \frac{4\mathrm{k_B T}\pi^2 \mathrm{e}^2}{\mathrm{h}^2} \sigma'(\mathrm{t}) \right\} \quad (5)$$

where T is the absolute temperature, σ'(t) is the mass-weighted covariance matrix , and R, k_B, and *h* are the ideal gas, Boltzmann, and Planck constants, respectively. Entropy values obtained with this approach are necessarily dependent on the simulation length (*t*), but are expected to tend to a limit entropy S_∞ for long enough sampling times (which depends on the particular system and must be empirically determined). In this context, the following empirical equation has been proposed[53,54], where S_∞ and α represent fitting parameters:

$$\mathrm{S_{conf}(t)} = \mathrm{S_\infty} - \frac{\alpha}{\mathrm{t}^{2/3}} \quad (6)$$

To ensure sampling time independence on our analysis, in this work, the Schliter entropy values were calculated for each simulation step, using CPPTRAJ[55] to compute σ'(t), and equation 6 was fitted to these values. The procedure was repeated for the five independent MD trajectories of CoA and CoA-Mg^{2+} complex, considering only CoA atom coordinates.

Conformational analysis with the Density Peaks Advanced clustering method

The DADApy[56] library was employed to identify stable conformations of CoA and the CoA-Mg^{2+} complex, with the Density Peaks Advanced[57] clustering method. The analysis was performed using 62500 frames belonging to the combined 2.5 μs long trajectories (water molecules were stripped with CPPTRAJ). To avoid performing the clustering analysis in Cartesian coordinates, which would yield a highly dimensional space and would be possibly redundant, we considered the space formed by a selection of dihedral angles. The selected set contained a total of 19 dihedral angles, associated with the rotation of bonds from the cysteamine tail to the ribose moiety, and is further illustrated in the next section. Therefore, our dataset was composed of the value of each of these 19 dihedral angles, for each analyzed frame. The clustering analysis was carried out with the density peaks advanced method, as implemented in the DADApy library, which employs free-energy-based ideas to find 'peaks' in the probability density (density peaks) of the dataset. This way, points belonging to the same cluster are expected to not only be close from each other in the selected space, but also to have similar free energies. The approach consists in an initial search for all local maxima of the probability

density and a further statistical significance analysis of each density peak localized. If a certain peak is considered to be statistically significant, it is considered a cluster center. Otherwise, it is merged to another peak. The statistical confidence interval is modulated by a parameter Z, which is an adjustable parameter. Lower values of Z lead to a larger number of clusters, but with lower statistical significance. In this work, we set this parameter to 4.0, as this value retrieved a reasonably stable clustering of random selections of the data (the effect of this parameter will be further discussed below, in the results section). Additionally, the density peaks advanced method requires an estimation of the Intrinsic Dimension[58] (ID) of the dataset, which can be understood as the minimum number of coordinates that conserves the same information as the full (in this case, 19-dimensional) space. This estimation was performed with the two nearest neighbors[59] (2NN) estimator, that is also implemented in the DADApy library, by searching for a *plateau* in the evolution of the ID with the scale of variations considered in the 2NN method. In our case, the ID was determined to be 6 both for CoA and CoA-complex datasets. For further explanations of these methods, we refer the readers to the original papers. The clustering analysis was performed by directly analyzing the mentioned trajectories as AMBER netcdf[60] files with an in-home automatization script of this protocol that uses the DADApy and ParmEd[61] libraries (available at https://github.com/JonathanSemelak/D-clust).

Finally, for the visualization of the clustering results, we used the Uniform Manifold Approximation and Projection[62] (UMAP) method, which yields a low-dimensional projection of a high-dimensional dataset, aiming to preserve its topography throughout the dimensionality reduction process. The results were then represented as scatter-plots on two-dimensional UMAP projections, and colored by cluster assignment or by selected interatomic distances obtained with CPPTRAJ.

Results and discussion

Thermodynamics parameters of CoA binding to Mg^{2+}

Isothermal calorimetric titration of CoA with Mg^{2+}

The interaction between Mg^{2+} and CoA was first explored by ITC at pH 7.2 and 25°C. For this, a solution of CoA was titrated with Mg^{2+} and the released heat due to the binding process was measured (**Figure S1**). It can be observed that the reaction is endothermic indicating that the driving force for the association process is the entropy change.

The area under each titration peak in the thermogram was calculated and represented as a function of the corresponding $[Mg^{2+}]_T$ / $[CoA]_T$ ratio (**Figure 2**). The same procedure was repeated using two other initial $[CoA]_T$ at the same pH and temperature (Figure 2B and 2C) and different binding models were assayed obtaining the best fit with the identical and independent sites model. **Table 1** shows the best fit values of the model parameters.

Table 1. Thermodynamic parameters of CoA binding to Mg^{2+} at 25°C.					
	n	K_a (M^{-1})	ΔH°' (kcal/mol)	ΔG°' (kcal/mol)[a]	-TΔS°' (kcal/mol)[b]
pH 7.2	1.07 ± 0.03	537 ± 20	1.17 ± 0.04	-3.72 ± 0.03	-4.89 ± 0.07
pH 7.8	0.99 ± 0.01	312 ± 7	1.85 ± 0.04	-3.40 ± 0.02	-5.25 ± 0.06
(a) calculated as $\Delta G^{\circ\prime} = - RT \ln K_a$; (b) calculated as $-T\Delta S^{\circ\prime} = \Delta G^{\circ\prime} - \Delta H^{\circ\prime}$					

The obtained binding stoichiometry was 1:1, and titration up to a mole ratio of 10:1 does not show any evidence of additional binding sites (**Figure 2C**). Because of the 1:1 stoichiometry, the microscopic association constant in equation 2 is equal to the thermodynamics (macroscopic) association constant K_a. As was mentioned, the binding process is entropically-driven, exhibiting ΔH°' and -TΔS°' values of 1.17 ± 0.04 and -4.91 kcal/mol, respectively. An endothermic and entropically-driven binding process is in agreement with previous reports for ATP-Mg^{2+} and UTP-Mg^{2+} complexes.[22,26] On the other hand, the positive values for the binding enthalpies indicate that the association constants will increase at higher temperatures.

To further characterize the interaction between Mg^{2+} and CoA, similar experiments were run at pH 7.8 in the presence of 120 mM KCl (**Figures 2D**, **2E** and **2F**). These conditions were selected resembling the pH and ionic composition of the mitochondrial matrix.[63,64] It can be observed that the process is still entropically driven, with a stoichiometry 1:1 and an association constant somewhat smaller than that measured at pH 7.2.

Considering the estimations of free Mg^{2+} and reported non-acyl CoA concentrations[18,19], and a mitochondrial temperature[65] of about 54°C, the expected concentration of CoA-Mg^{2+} are in the range of 0.32-1.28 mM in mitochondria. In the case of the cytosol, the concentrations of the complex calculated at a physiological temperature (37°C) were ≤ 50 µM, which still represents an important fraction of non-acyl CoA (10-40% of non-acyl CoA would bind Mg^{2+} both in the cytosol and mitochondria). This information is summarized in Table 2. Note that the reported non-acylated CoA concentrations do not discriminate between free CoA and CoA bound to macromolecules (nor in oxidized states). For this reason, we also report the ratio [CoA-Mg^{2+}]/free [CoA], as can be directly obtained from the association constant and free Mg^{2+} concentration, without any approximation in the mass balance of CoA. Although we did not determine the binding affinity of acetyl- or other acyl-CoAs for Mg^{2+}, considering the main atoms involved in the process, we propose that these molecules also bind Mg^{2+} using a similar mechanism as non-acyl CoA.

Table 2. Estimated concentrations for CoA-Mg^{2+} complex.

	[CoA] (mM)[18,19]	free [Mg^{2+}] (mM)[a]	[CoA-Mg^{2+}]/free [CoA][b]	[CoA-Mg^{2+}] (mM)[c]
mitochondria (25°C)	2.55-3.35	0.35-1.5	0.11-0.47	0.25-1.07
cytosol (25°C)	0.05-0.09	0.37-2.1	0.19-0.80	0.008-0.047
mitochondria (54°C)[d]	2.55-3.35	0.35-1.5	0.14-0.62	0.32-1.28
cytosol (37°C)[d]	0.05-0.09	0.37-2.1	0.21-0.92	0.009-0.050

(a) The estimated concentration of free Mg^{2+} varies depending on the particular tissues and conditions and is estimated to be 1-3% of the total concentration[66–68]; (b) Calculated as K_a/free [Mg^{2+}]; (c) Estimated assuming no other species compete with Mg^{2+} for free CoA; (d) Since the exact temperature of the mitochondrial matrix is still a subject of debate and varies with metabolic conditions and cell types [69–71], we decided to report also the results for 25°C (the temperature at which the calorimetry determinations were done) which were quite similar although values were slightly lower. The association constants at these temperatures were estimated with the Van't Hoff equation as $\ln(K_a(T_2)/K_a(T_1))=(\Delta H°'/R)(1/T_1-1/T_2)$.

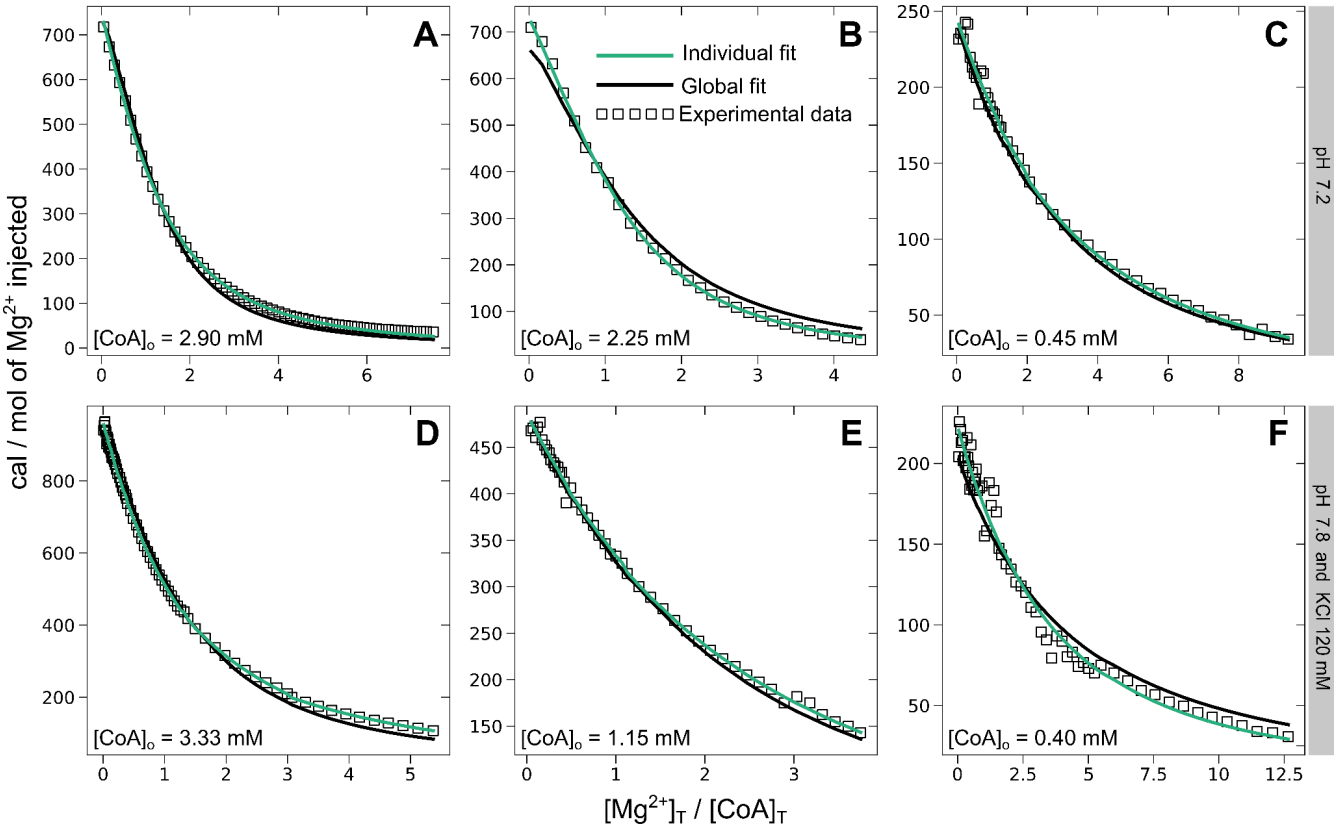

Figure 2. *Calorimetric titration curves for the interaction between CoA and Mg^{2+}.* $MgCl_2$ and CoA solutions were prepared in 100 mM Tris-HCl pH 7.2 at 25 ºC (panels A-C), or 100 mM Tris HCl pH 7.8 at 25 °C, 120 mM KCl (panels D-F). Three dilutions were prepared in each buffer and CoA concentrations were measured as described in methods. The initial concentrations ($[CoA]_{T,0}$) were: 2.90 mM (A), 2.25 mM (B), 0.45 mM (C), 3.33 mM (D), 1.15 mM (E), 0.40 mM (F). Titrations were performed as described and the heat absorbed after each Mg^{2+} injection was calculated and expressed as a function of the corresponding $[Mg^{2+}]_T$ / $[CoA]_T$ ratio. Continuous black lines are the graphical representation of the global fitting of a model of identical and independent sites to each set of experimental data. The best fit values of the parameters are indicated in Table 1**.** The individual fit to each panel data is shown by green lines.

Conformational entropy change

According to the ITC results indicated above (**Figure 2**), the overall binding process of Mg^{2+} to CoA is entropically driven., i.e., it involves an increase in the entropy of the system. Without considering the solvent degrees of freedom, a binding process necessarily involves a loss in translational entropy. Thus, the positive entropy gain observed experimentally must result from some other contribution. To obtain a semi-quantitative estimation of the configurational entropy change, we performed a computational calculation of the configurational entropy of the CoA atoms in the complex compared with free CoA (**Figure 3**). An extrapolation to infinite sampling according to equation 6 yields a $-T\Delta S_{conf}$ value of 4.2 kcal/mol, ruling out increased configurational entropy as the cause of the negative $-T\Delta S$ obtained experimentally. This is consistent with the expected increase in rigidity associated to Mg^{2+} binding. Furthermore, this result supports that the origin of the positive entropy change experimentally obtained should be related with solvent degrees of freedom contributing to the total $-T\Delta S$ with about -9.2 kcal/mol). This idea is consistent with the entropically driven binding of Mg^{2+} to diphosphate-containing groups being previously attributed to the entropy gain of water molecules from the Mg^{2+} solvation shell.[38]

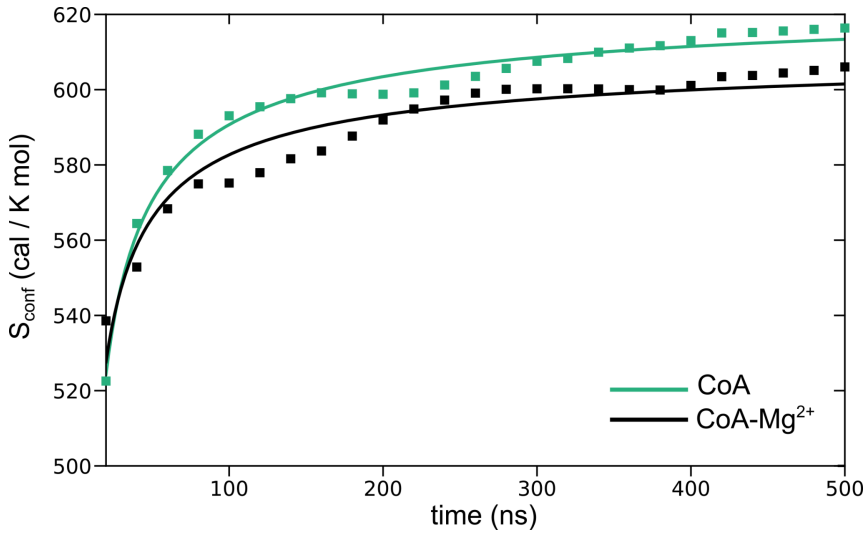

Figure 3. *Configurational entropy of free CoA and CoA-Mg^{2+} complex, obtained from molecular dynamics simulation.* Only CoA atoms' coordinates were used to compute the mass-weighted covariance matrix. The results correspond to the average of five independent 500 ns long MD simulations. The fitting of equation 6 retrieves S_∞ and α values of (625 ± 1) cal/K mol and (616 ± 1259) cal $ns^{2/3}$/ K mol, respectively for CoA, and S_∞ and α values of (611 ± 3) cal/K mol and (743 ± 448) cal $ns^{2/3}$/ K mol, respectively for CoA-Mg^{2+}. These results correspond to a $-T\Delta S_{conf}$ value of 4.2 kcal/mol in the limit of infinite sampling.

CoA-Mg^{2+} binding mode elucidated from NMR experiments and molecular dynamics simulations

A paramagnetic metal ion impurity induces selective line broadening in the NMR spectra

Initially, we prepared a 3.2 mM solution of CoA in 50 mM Tris buffer pH 7.2 containing 5% D_2O. Detected ^1H chemical shifts are in agreement with the reported for CoA.[40,72] However, notably, some CoA signals appear significantly broadened, while others are missing from the ^1H NMR spectrum, and no signal is observed in the ^{31}P NMR spectrum (**Figure 4A**). Signals of hydrogens **a8**, **a5'**, **a4'**, and **p10** and the three phosphorus atoms **Pp10, Pa5'**, and **Pa3'** are broadened beyond detection in the NMR spectra, and hydrogen signals **a1'**, **p8** and **p9** are detected but significantly broadened (**Figure 4B**, as **a2'** and **a3'** ^1H signals are overlapped to the water signal, we do not have information for these positions).

We hypothesized that the observed broadening could be due to the presence of traces of a paramagnetic metal ion in the sample that interacts with CoA. Indeed, the paramagnetic broadening effect is usually very sensitive, and the presence of a small amount of a paramagnetic ligand very often causes severe broadening in the NMR signals of testing samples.[73,74] For example, an analogous effect was reported in the case of α,β-methyleneadenosine triphosphate in complex with *Escherichia coli* MutT enzyme and Mg^{2+} upon Mn^{2+} addition.[75] To verify our hypothesis, we performed Mg^{2+} displacement experiments by adding $MgCl_2$ to the CoA NMR sample to obtain final magnesium concentrations of 200, 350, and 500 mM. The CoA signals exhibiting line broadening in the original sample are progressively sharpened as Mg^{2+} is added to the solution (**Figure 4C**). Sharpening occurs for all the broadened CoA signals but is more accentuated for those signals that had been broadened beyond detection. This feature supports the presence of paramagnetic metal ion (such as Mn^{2+}, Fe^{2+}, or Cu^{2+}) traces interacting with CoA, which is displaced by the increasing concentrations of Mg^{2+}, and indicates that the interaction with magnesium involves the atoms whose signals are broadened in the presence of the paramagnetic ion (**Figure 4B**).

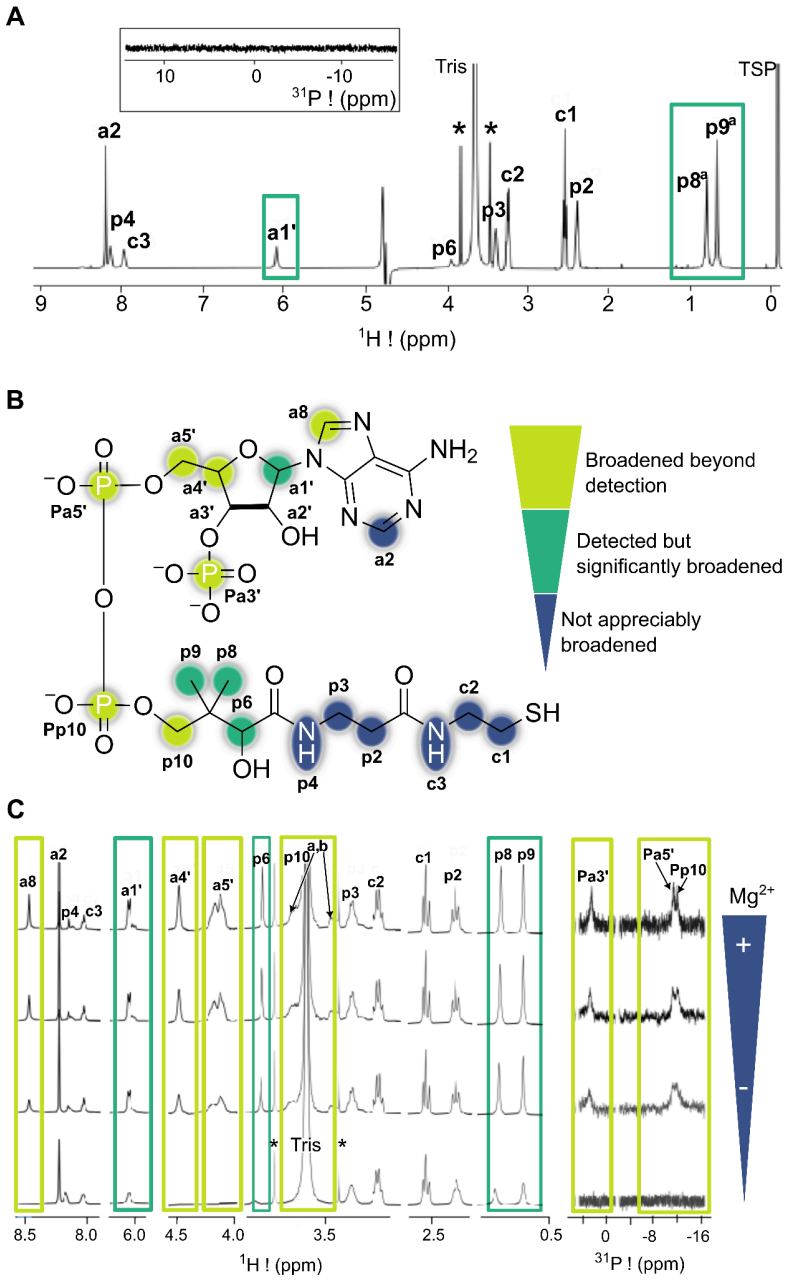

Figure 4. *Selective line-broadening and displacing experiments with Mg^{2+}*. **A.** ^{1}H and ^{31}P (inset) NMR spectra of a 3.2 mM CoA solution in 50 mM Tris pH 7.2, not previously pre-treated with Chelex. Several signals are missing from the spectra and others, boxed with a green line, are significantly broadened. (**B**) Positions whose signals are broadened beyond detection (lime-yellow), detected but significantly broadened (green), and not appreciably broadened (blue), are mapped to the CoA atoms with a color scale. (**C**) ^{1}H and ^{31}P NMR spectra in the absence of $MgCl_2$, and the presence of 200, 350, and 500 mM $MgCl_2$ (from bottom to top), showing the progressive sharpening of the CoA signals upon magnesium interaction. Signals originally broadened beyond detection and signals detected but

broadened are boxed with lime-yellow and green lines, respectively. The signal of Tris is indicated and its ^{13}C satellites are shown with asterisks.

CoA chemical shift perturbation upon Mg^{2+} *interaction*

To avoid paramagnetic broadening, in all the subsequent samples, the buffer was pretreated with Chelex 100 to remove possible traces of divalent metal cations. **Figure S2** shows the ^{1}H, ^{31}P, and ^{1}H-^{13}C HSQC NMR spectra obtained for a 5 mM CoA solution, and **Table S1** reports the ^{1}H, ^{13}C, and ^{31}P chemical shift assignments of the reduced and oxidized forms of CoA (CoA-SH and CoA-S-S-CoA, respectively), which are in line with previous studies.[40,72,76,77] Initially, <5% of CoA was oxidized, but we observed that CoA oxidation proceeded in the NMR tube during experiments acquisition. Eight hours after sample preparation, 30% of CoA was oxidized (not shown). For the reduced CoA-SH, the ^{13}C signals of **c1** and **c2** are expected around 24 and 42 ppm, respectively; on the other hand, for CoA-S-S-CoA, **c1** is expected to yield a ^{13}C chemical shift around 37 ppm, and **c2** around 38 ppm (**Figure S3**). This way, the chemical shifts of **c2** and **c1** carbons for the main form of CoA are diagnostic of the reduced form.

To investigate the interaction of CoA with magnesium, we added $MgCl_2$ to a 5 mM CoA sample in two steps to final magnesium concentrations of 50 and 150 mM. The corresponding ^{1}H-^{13}C HSQC NMR spectra are shown in **Figure S4**. We observed progressive changes in the chemical shifts of some NMR signals, confirming the interaction between Mg^{2+} and CoA. Moreover, this observation shows that, in our experimental conditions, the exchange between the CoA-Mg^{2+} complex and free CoA is fast in the NMR time scale. Interestingly, while in the absence of Mg^{2+} the two hydrogens **a5'** exhibit the same chemical shift, when Mg^{2+} is added, the signals of these two diastereotopic hydrogens are different (see **Figure S4A**). Possibly, in the CoA-Mg^{2+} complex, the motion of this part of the molecule is somewhat restricted (consistently with the negative ΔS_{conf} value determined for the binding process), providing a different chemical environment for each of **a5'** hydrogens.

Figure 5 shows the combined ^{1}H-^{13}C and ^{31}P chemical shift perturbation (CSP) values observed for CoA upon Mg^{2+} interaction, determined according to equation 3 (and as a simple difference for ^{31}P signals), using chemical shift values extracted from the NMR spectra shown in **Figure S4**. The most perturbed signals are those corresponding to positions **a8**, **a3'**, one of the **a5'** hydrogens, as well as the three phosphorus atoms **Pa3'**, **Pp10**, and, to a lesser extent, **Pa5'**. In contrast, **a2**, **a2'** and **a4'**, one of **p10** hydrogens, **p8**, **p2**, and **p3**, **c1**, and **c2** positions are almost not perturbed at all by magnesium interaction, while positions **a1'**, the other **a5'** and **p10** hydrogens, **p9**, and **p6** are moderately disturbed. These results show that the chemical environment of selected fragments is modified upon Mg^{2+} binding, suggesting that the interaction may involve the nucleotide moiety of CoA and the region of pantothenate close to the phosphate group. On the other hand, the cysteamine and β-alanine moieties seem not to be involved in the metal interaction. The three phosphate signals are also perturbed upon magnesium binding, consistently with the phosphate groups being implicated in the

metal complex formation. We observed a high field shift of the three phosphate signals, as well as line width broadening upon magnesium addition, which is more accentuated for **Pa3'**, suggesting a fast-intermediate exchange between the metal complex and free CoA at the ^{31}P frequency under the experimental conditions employed (**Figure S4B**).

The progressive perturbations of the NMR signals observed with 1:10 and 1:30 equivalent ratios of CoA:Mg^{2+}, at a 5 mM CoA concentration, allow us to provide an additional rough estimation (since it is an estimation based only on three points) of the K_a for Mg^{2+} binding, which results in the 10^2-10^3 M^{-1} range (**Figure S5**), consistent with the 537 M^{-1} value determined by ITC at the same experimental pH.

Oxidized CoA also interacts with Mg^{2+}, apparently involving the same region of CoA and with a similar affinity to the reduced form (not shown).

Importantly, the signals that experience an increased paramagnetic broadening due to the metal impurity are coincident with the signals that undergo significant CSP values upon Mg^{2+} interaction, confirming the interaction of Mg^{2+} with CoA occurs in the region of the molecule involving the three phosphates, the segment of pantothenate adjacent to the phosphate group, the ribose moiety (positions **a3'** and **a5'**), and the hydrogen in position **a8** of adenine.

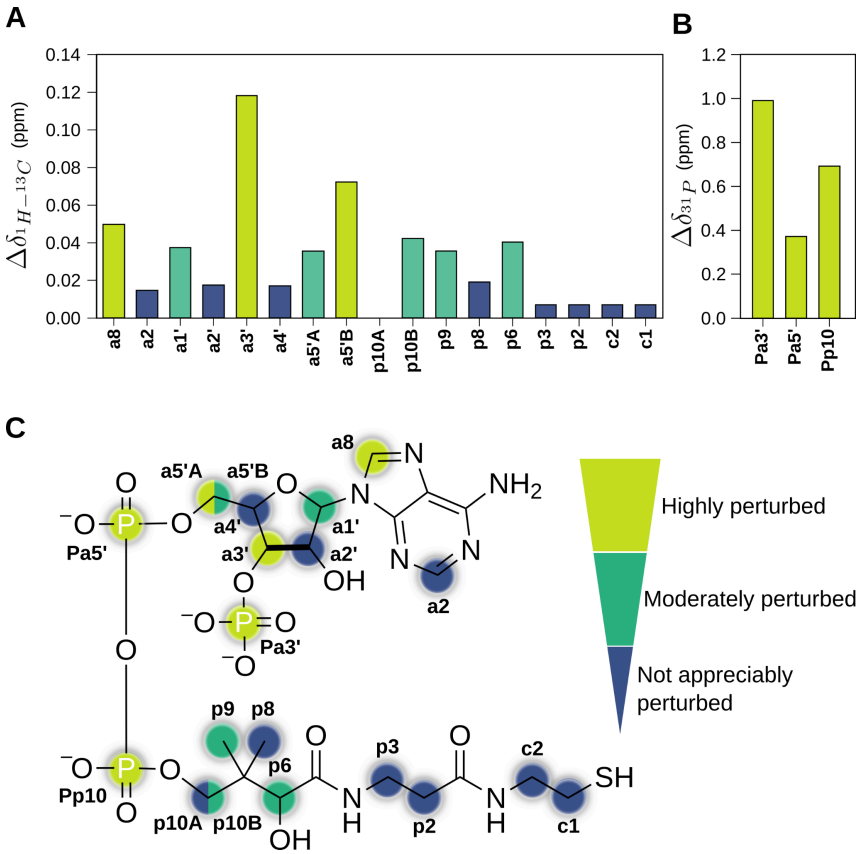

Figure 5. *CoA chemical shift perturbations upon Mg^{2+} interaction.* Combined ^{1}H and ^{13}C (**A**) and ^{31}P (**B**) CSPs observed for a 5 mM CoA solution in Chelex-treated 50 mM Tris pH 7.2 upon the addition of 30 equivalents of $MgCl_2$. Results are mapped in the chemical structure of CoA in (**C**). We should notice that while **a2'** and **a3'** are not captured in the 1D ^{1}H spectra due to water suppression (**Figures 4** and **S2A**), they are detectable in the 2D ^{1}H-^{13}C HSQC spectra (**Figures S2C** and **S4A**).

Conformational landscape of free CoA

The NMR experiments exhibited that the CoA conformational landscape is perturbed upon Mg^{2+} binding. This observation could be not only because of the presence of the ion itself but also because of restrictions that binding imposes on the torsional freedom of CoA atoms, making it prone to explore different conformations and, subsequently, inducing different local environments for some of its atoms. In this section, we use the MD trajectories from which we computed the configurational entropy change, but this time to extract structural and dynamical data that would complement the insights from NMR experiments.

The presence of Mg^{2+} necessarily restrains some of the torsions involving **Pa5'** and **Pp10** (because they are directly involved in the coordination), however, the effect could be extended to other torsions of the flexible tail integrated by the cysteamine and 4-phosphopantothenate units, as well as part of the 3',5'-diphosphate. This way, to analyze the configurational changes induced upon Mg^{2+} binding, we considered the space formed by a selection of dihedral angles from the CoA tail, illustrated in **Figure 6A**. Additionally, to conduct the analysis in an unbiased approach, we employed the density peaks advanced clustering algorithm, an unsupervised learning technique. This method allowed us to identify clusters searching zones of high density in the selected space, grouping structures that are similar in terms of the selected dihedral angles. The results obtained are shown in **Figure 6B**, projected on UMAP reduced dimensions for visualization. In **Figures S6** and **S7** we justify the choice of a Z parameter of 4.0 for this analysis.

It can be seen that data points belonging to the same cluster are close to each other in the reduced dimensions space, as expected for a transformation that aims to conserve the topology structure of the original space. Additionally, it is noteworthy that most of the population lies in a small number of clusters. For example, above 90% of the population falls in clusters I to III, in the case of free CoA, and in clusters I' and II', in the case of CoA-Mg^{2+} complex.

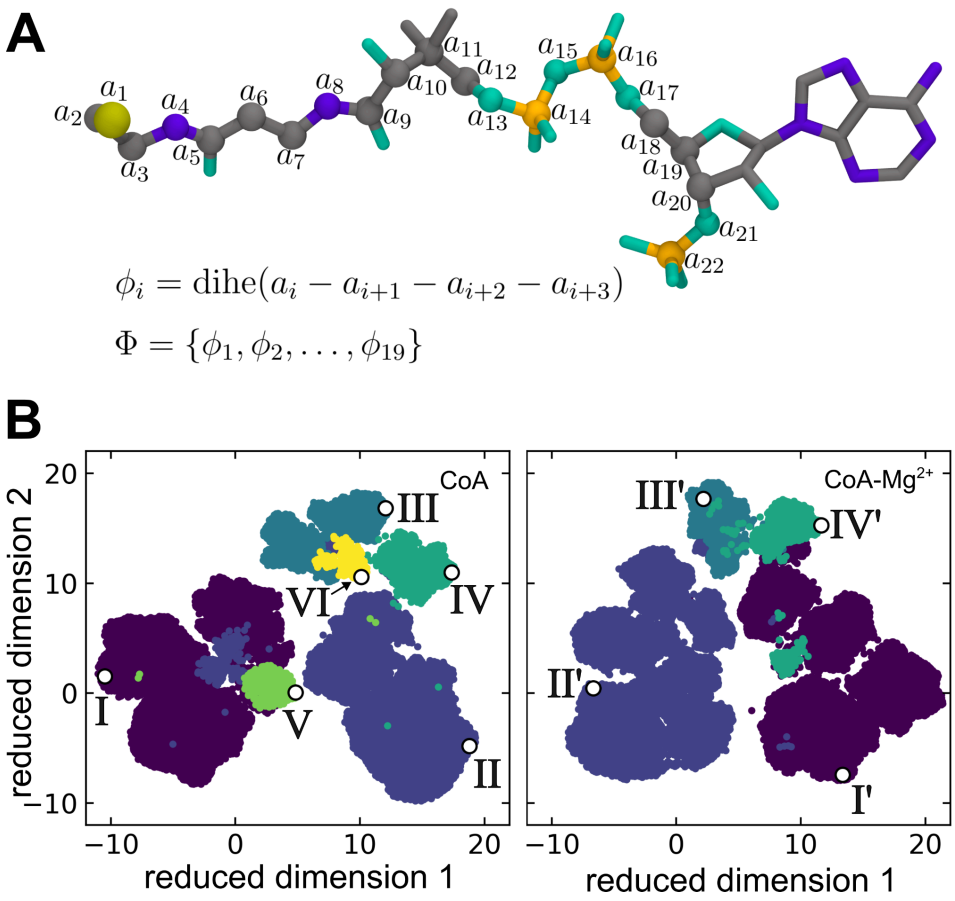

Figure 6. *Clustering results of selected dihedral angles from CoA with the* density peaks advanced *method.* (**A**) The heavy atoms of the CoA molecule are shown, along with the definition of the dihedral angles integrating the space **Φ**, in which the clustering was performed. (**B**) Scatter plot of a 2D UMAP reduced dimensions of the data set, according to cluster assignment. The white circles indicate the positions of the cluster centers. The clusters are labeled from I to VI (CoA) and I' to IV' (CoA-Mg^{2+} complex) by decreasing population. Populations (%) from I to VI are 42.5, 41.5, 7.9, 5.0, 1.9 and 1.1, respectively. Populations (%) from I' to IV' are 45.2, 45.0, 5.3 and 4.4, respectively.

In **Figure 7** we show the structures belonging to the centers of the most populated clusters found by the density peaks advanced method. The same, but including every cluster, is shown in **Figures S8** and **S9**. These cluster centers should be interpreted as representative points of the collection of structures that constitutes each cluster. While the clustering analysis was performed in a space consisting of only dihedral angles, the cluster centers exhibit unique hydrogen bond (HB) intramolecular interactions. This correlation between clustering with the density peaks advanced method in a space of dihedrals and a space of intramolecular distances has been previously observed.[56] Moreover, while here we are focusing our analysis in the clusters centers, in **Figures S10** and **S11**, the discussion is extended by coloring the data in the reduced dimensions according to selected intramolecular distances. In **Figures 7A** and **S8**, we show the results for free CoA. It can be

seen that in each center, the phosphate group of **Pa3'** interacts with the -OH group from the ribose ring. This interaction can occur with the phosphate group pointing towards the -OH group, or as in the case of cluster center I, through the oxygen atom between phosphorus **Pa3'** and the ribose ring. Interestingly, among the phosphates forming the diphosphate group (**Pa5'** and **Pp10**), only **Pa5'** establishes an intramolecular HB. From a more general perspective, only HB interactions between the cysteamine vs adenosine 3',5'-diphosphate and 4-phosphopantothenic acid vs adenosine 3',5'-diphosphate are observed. In other words, HB interactions between the cysteamine and 4-phosphopantothenic acid groups seem to be prohibited (or at least not thermodynamically favored), and so is the bending of the tail towards itself (that would be stabilized by such interactions).

In a previous work[30], we examined the CoAlation site of known 3D structures of CoAlated proteins (i.e. covalently bound to CoA by a disulfide bond) and identified three main types of CoAlated proteins, showcasing that CoA is a very flexible molecule (exhibiting extended and bent forms) that is able to: 1) reach cysteine residues buried within the protein structure (and so fitting in specific pockets); 2) reach solvent exposed cysteine residues, while still being attached to hydrophobic pockets; and 3) fit in the pocket/groove formed by two protein subunits. Interestingly, when we compare these observations with the conformational landscape we observed for free CoA in aqueous solution (this work), it seems that the environment provided by protein residues of CoAlation sites is able to push the limits of CoA flexibility.[76] For example, in the case of the CoAlated histone acetyltransferase p300/CBP associated factor (PDB ID 4NSQ[78]), the cysteamine unit is particularly bent towards the 4-phosphopantothenic acid group, in a way that we did not observe for CoA in aqueous solution. This observation highlights that in the case of such a flexible molecule like CoA, the delicate balance between inter and intramolecular interactions could tune its conformational landscape, allowing it to fit in different types of protein pockets.

Mg^{2+} binding imposes changes in the conformational landscape of CoA

In the presence of a single Mg^{2+} ion, the conformational landscape of CoA changes to that of **Figures 7B** and **S9**. Notably, CoA retains its flexibility even when bound to Mg^{2+} , as evidenced by the RMSD plot in **Figure S12** and the attached movies in the Supplementary Material.

Regarding the clustering analysis, the first noticeable aspect is that the binding mode is split almost 50% with the phosphate group **Pa3**' pointing towards the Mg^{2+} ion (like in clusters II' and III'), and 50% in which only **Pa5'** and **Pp10** interact with it. This is illustrated by the histograms shown in **Figures 7** and **S9**, where structures belonging to clusters II' and III' exhibit a narrow peak around 4.5 Å in the distance between the Mg^{2+} ion and phosphorus **Pa3'**. This result is in agreement with the conclusion drawn from the NMR experiment that Mg^{2+} ion interacts with the three phosphate groups of CoA. Moreover, it provides the additional information that while the three phosphate groups are involved in the binding of Mg^{2+}, only **Pa5'** and **Pp10** participate consistently in the interaction, and **Pa3'** only half of the time, through Mg^{2+} coordination waters. This could eventually explain the larger

broadening of the **Pa3'** signal in comparison with those of **Pa5'** and **Pp10,** observed in the NMR experiments (**Figure 4B**). The involvement of phosphate **Pa3'** in the coordination of Mg^{2+} and the associated change in its chemical environment is especially interesting, as it has been shown to play a key role in the catalytic mechanism of human medium-chain acyl-CoA dehydrogenase.[79]

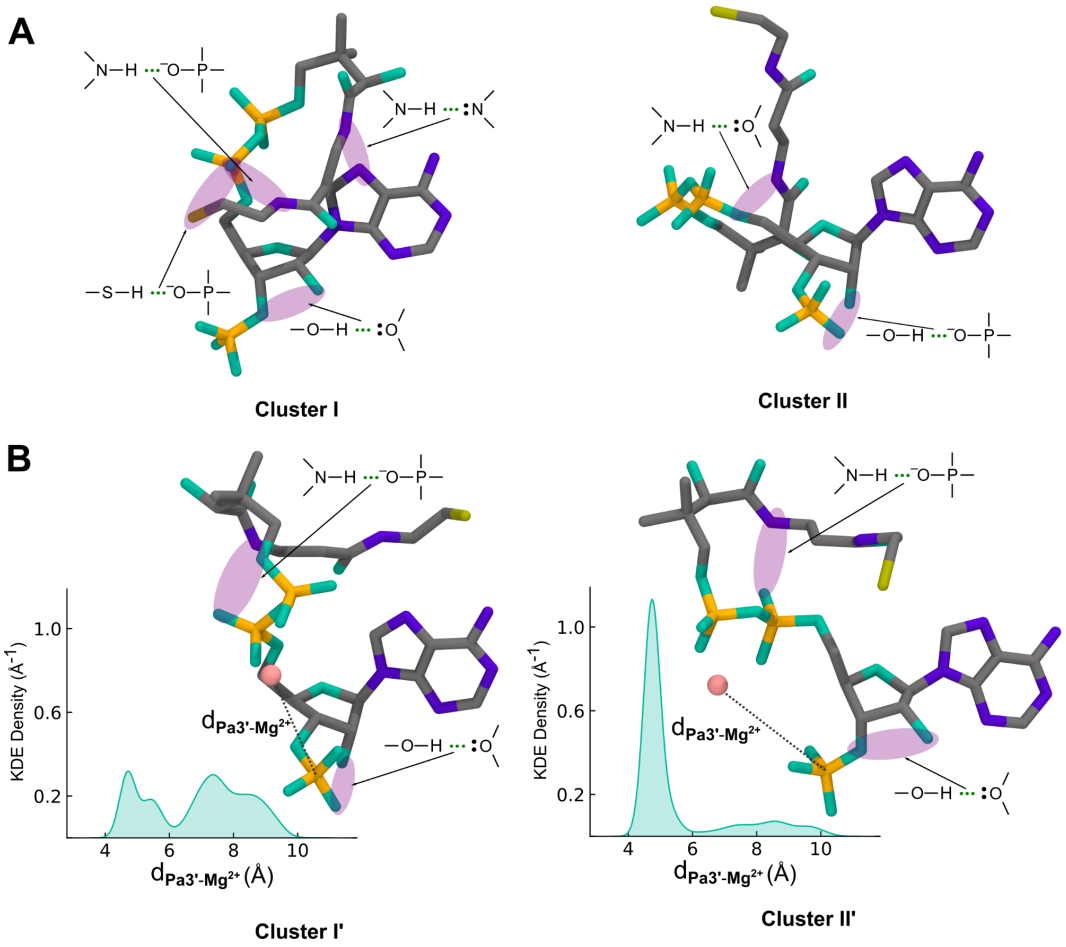

Figure 7. *Structures of centers of the most populated clusters found by the advanced density peaks method.* (**A**) Centers of clusters I and II (CoA). (**B**) Centers of clusters I' and II' (CoA-Mg^{2+}) along with histograms (in the form of KDE Density plots) showing the distribution of the distance between Pa3' and the Mg^{2+} ion along the frames of each cluster. Only heavy atoms of CoA are shown for simplicity. Intramolecular HB are highlighted in purple (criterium: acceptor-hydrogen distance lower than 2.5 Å). Carbon, nitrogen, oxygen, sulfur and phosphorus atoms are shown in gray, violet, green, yellow, and orange, respectively.

The binding mode of the CoA-Mg^{2+} complex differs from that proposed for the analogous CoA-Mn^{2+} complex.[24] Based on molar paramagnetic relaxation rates obtained from ^{1}H NMR experiments, it has been proposed that phosphate **Pa3'** does not participate in the Mn^{2+} coordination, and that the -OH group from position **p6** and the adenine ring are directly involved in the Mn^{2+} coordination. With this information, a highly folded structure was proposed for the CoA-Mn^{2+}

complex in aqueous solution, so it could satisfy simultaneously that the distances between hydrogens of positions **p6**, **a2** and **a8** and the Mn^{2+} were 4.1- 4.6 Å. In our case, the average distance between Mg^{2+} and hydrogen **p6** is about 6 Å and the -OH group never interacts with the Mg^{2+} ion directly. On the other hand, the average distances between Mg^{2+} and hydrogens **a2** and **a8** are about 11 and 7 Å, respectively, being significantly asymmetric (and also consistent with **a8** experiencing a larger paramagnetic broadening). The binding of Mn^{2+} to CoA may induce different modifications in the CoA conformational landscape. For example, while that could not be the only contributing factor, it has been reported that Mn^{2+} promotes the activity of acetyl-CoA carboxylase in conditions in which Mg^{2+} is unable to do so.[80] In the same line, our study on free CoA and CoA-Mg^{2+} dynamic structures strongly supports that even when complexed, CoA remains a very flexible molecule, and so a structure in which the distances between Mg^{2+} and hydrogens **p6**, **a2**, and **a8** are about 4.1- 4.6 Å simultaneously, is unlikely to be a predominant conformation.

Finally, as the sulfur atom of CoA constitutes the nucleophilic center that leads CoA to form disulfide bonds to different proteins and is also the target of acyl-CoA synthetases[81], it may be worth noticing that the binding of Mg^{2+} and the subsequent population of conformations represented by cluster II', that is characterized by the tail bending towards the diphosphate group of CoA (**Figure 8**), may perturb the chemical environment of the sulfur atom from the -SH group. Whether this change could lead to significant modifications of its nucleophilicity or its acidity is yet to be determined. Nevertheless, within the limitations of the chosen forcefield, the combination of clustering analysis and NMR experiments suggest that the binding of Mg^{2+} to CoA induces changes in the local environment of relevant fragments of CoA, regardless of their distance to the binding site.

In spite of the reported 3 fold higher affinity constant of Mn^{2+} compared with Mg^{2+} for CoA (910 M^{-1} at pH 8)[82], and due to the much lower concentration of Mn^{2+} in the mitochondria (approximately 3 µM as labile low molecular weight species)[7], Mn^{2+} would not constitute an important competitor for Mg^{2+} binding to CoA under physiological conditions. Similarly, the basal concentration of Ca^{2+} in resting mitochondria is considerably lower than that of Mg^{2+} (100-200 nM, although it can increase considerably under stimulation in some mitochondrial microdomains)[7] and therefore it is unlikely that Ca^{2+} can compete with Mg^{2+} binding to CoA at least under basal conditions, particularly if the affinity constant tendency among nucleotides such as ATP where the affinity of Ca^{2+} is lower than that of Mg^{2+} is maintained in the case of CoA.[83]

The consequences of the interaction of CoA with Mg^{2+} on the different functions of the coenzyme are expected to largely depend on the particular proteins involved. For example, Mg^{2+} competes with glucose 6-phosphate dehydrogenase for CoA binding, and therefore releases CoA-mediated protein inhibition.[29] Mg^{2+} also inhibits the binding of CoA to acetyl CoA carboxilase, in this case leading to a decrease of CoA-dependent protein activation.[84] Furthermore, the crystal structure of the Ser/Thr kinase aurora kinase A in complex with CoA shows that in this case the

interaction is with CoA and Mg^{2+}.[85] It is tempting to speculate that for those proteins interacting with CoA at a nucleotide binding site, and since nucleotides usually bind proteins in complex with Mg^{2+}, CoA-Mg^{2+} probably has an enhanced affinity compared with CoA, leading to a greater competitive inhibition. However, as indicated above, these effects should be tested on an individual protein basis.

Conclusions

The combination of ITC experiments, NMR spectroscopy and molecular dynamics simulations allowed us to provide the first structural and thermodynamic characterization of Mg^{2+} binding to CoA in aqueous solution. We found that Mg^{2+} binds to CoA in a 1:1 stoichiometry with association constants of (537 ± 20) M^{-1} at pH 7.2 and (312 ± 7) M^{-1} at pH 7.8 and composition resembling the mitochondrial matrix. Based on this affinity, the fraction of CoA bound to Mg^{2+} is estimated to be significant both in the cytosol and the mitochondrial matrix. We also determined that the binding is entropically driven, and the associated entropic gain seems to be solvent-related. Furthermore, we mapped the Mg^{+2} interaction sites in the CoA molecule and found that the coordination occurs mainly through the diphosphate group, with the phosphate group from the ribose ring participating only indirectly in the binding, about half of the time, and through Mg^{2+} coordination waters. Finally, MD calculations showed that the conformational landscape of CoA is severely modified upon Mg^{2+} binding, inducing changes in the chemical environment of CoA atoms, regardless of their distances to the binding site. However, even when complexed to Mg^{2+}, CoA remains a highly flexible moiety.

Abbreviations List

CoA, coenzyme A; NMR, nuclear magnetic resonance; ITC, isothermal titration calorimetry; MD, molecular dynamics; ATP, adenosine triphosphate; UTP, uridine triphosphate; ADP, adenosine diphosphate; UDP, uridine diphosphate; HB, hydrogen bond.

Author contributions

JAS: Conceptualization, Data curation, Formal analysis, Investigation, Project administration, Software, Validation, Visualization, Writing - original draft, Writing - review & editing; **MG:** Conceptualization, Formal analysis, Investigation, Validation, Visualization, Writing - original draft, Writing - review & editing; **FLGF**: Conceptualization, Formal analysis, Investigation, Validation, Visualization, Writing - original draft, Writing - review & editing; **SDP:** Formal analysis, Software, Visualization, Writing - original draft, Writing - review & editing; **TAP:** Conceptualization, Formal analysis, Investigation, Validation, Visualization, Writing - original draft, Writing - review & editing; **AZ**: Conceptualization, Investigation, Project administration, Writing - original draft, Writing - review & editing; **IG:** Conceptualization, Writing - original draft, Writing - review & editing; **DAE:** Conceptualization, Project administration, Resources, Supervision, Funding acquisition, Writing - original draft, Writing - review &

editing; **MT:** Conceptualization, Formal analysis, Funding acquisition, Investigation, Project administration, Resources, Supervision, Writing - original draft, Writing - review & editing.

Founding Sources

This work was supported by Universidad de la República (grant Centros 2020, Espacio Interdisciplinario), the Agencia Nacional de Promoción de la Investigación, el Desarrollo Tecnológico,y la Innovación (grant PICT 2020-01828 and 2019-02768); Universidad de Buenos Aires (grant UBACYT 20020220200002BA), and Consejo Nacional de Investigaciones Científicas y Técnicas (grant 11220200102757CO and JAS's fellowship). Additional funding was obtained from Programa de Desarrollo de Ciencias Básicas (PEDECIBA), and Programa de Alimentos y Salud Humana (PAyS, IDB-R.O.U. 4950/OC-UR).

References

(1) Fatholahi, M.; LaNoue, K.; Romani, A.; Scarpa, A. Relationship between Total and Free Cellular Mg2+ during Metabolic Stimulation of Rat Cardiac Myocytes and Perfused Hearts. *Arch. Biochem. Biophys.* **2000**, *374* (2), 395–401. https://doi.org/10.1006/abbi.1999.1619.

(2) de Baaij, J. H. F.; Hoenderop, J. G. J.; Bindels, R. J. M. Magnesium in Man: Implications for Health and Disease. *Physiol. Rev.* **2015**, *95* (1), 1–46. https://doi.org/10.1152/physrev.00012.2014.

(3) Romani, A. M. P. Intracellular Magnesium Homeostasis. In *Magnesium in the Central Nervous System*; Vink, R., Nechifor, M., Eds.; University of Adelaide Press: Adelaide (AU), 2011.

(4) Ebel, H.; Günther, T. Magnesium Metabolism: A Review. **1980**, *18* (5), 257–270. https://doi.org/10.1515/cclm.1980.18.5.257.

(5) Long, S.; Romani, A. M. Role of Cellular Magnesium in Human Diseases. *Austin J. Nutr. Food Sci.* **2014**, *2* (10), 1051.

(6) Daw, C. C.; Ramachandran, K.; Enslow, B. T.; Maity, S.; Bursic, B.; Novello, M. J.; Rubannelsonkumar, C. S.; Mashal, A. H.; Ravichandran, J.; Bakewell, T. M.; Wang, W.; Li, K.; Madaris, T. R.; Shannon, C. E.; Norton, L.; Kandala, S.; Caplan, J.; Srikantan, S.; Stathopulos, P. B.; Reeves, W. B.; Madesh, M. Lactate Elicits ER-Mitochondrial Mg2+ Dynamics to Integrate Cellular Metabolism. *Cell* **2020**, *183* (2), 474-489.e17. https://doi.org/10.1016/j.cell.2020.08.049.

(7) Killilea, D. W.; Killilea, A. N. Mineral Requirements for Mitochondrial Function: A Connection to Redox Balance and Cellular Differentiation. *Free Radic. Biol. Med.* **2022**, *182*, 182–191. https://doi.org/10.1016/j.freeradbiomed.2022.02.022.

(8) Leonardi, R.; Zhang, Y.-M.; Rock, C. O.; Jackowski, S. Coenzyme A: Back in Action. *Prog. Lipid Res.* **2005**, *44* (2), 125–153. https://doi.org/10.1016/j.plipres.2005.04.001.

(9) Begley, T. P.; Kinsland, C.; Strauss, E. The Biosynthesis of Coenzyme A in Bacteria. In *Vitamins & Hormones*; Cofactor Biosynthesis; Academic Press, 2001; Vol. 61, pp 157–171. https://doi.org/10.1016/S0083-6729(01)61005-7.

(10) Mignani, L.; Gnutti, B.; Zizioli, D.; Finazzi, D. Coenzyme A Biochemistry: From Neurodevelopment to Neurodegeneration. *Brain Sci.* **2021**, *11* (8), 1031. https://doi.org/10.3390/brainsci11081031.

(11) Guertin, D. A.; Wellen, K. E. Acetyl-CoA Metabolism in Cancer. *Nat. Rev. Cancer* **2023**, *23* (3), 156–172. https://doi.org/10.1038/s41568-022-00543-5.

(12) Kresge, N.; Simoni, R. D.; Hill, R. L. Fritz Lipmann and the Discovery of Coenzyme A. *J. Biol. Chem.* **2005**, *280* (21), 164–166. https://doi.org/10.1016/S0021-9258(20)64101-1.
(13) Menzies, K. J.; Zhang, H.; Katsyuba, E.; Auwerx, J. Protein Acetylation in Metabolism — Metabolites and Cofactors. *Nat. Rev. Endocrinol.* **2016**, *12* (1), 43–60. https://doi.org/10.1038/nrendo.2015.181.
(14) Carrico, C.; Cruz, A.; Walter, M.; Meyer, J.; Wehrfritz, C.; Shah, S.; Wei, L.; Schilling, B.; Verdin, E. Coenzyme A Binding Sites Induce Proximal Acylation across Protein Families. *Sci. Rep.* **2023**, *13* (1), 5029. https://doi.org/10.1038/s41598-023-31900-5.
(15) Tsuchiya, Y.; Peak-Chew, S. Y.; Newell, C.; Miller-Aidoo, S.; Mangal, S.; Zhyvoloup, A.; Bakovic´, J.; Malanchuk, O.; Pereira, G. C.; Kotiadis, V.; Szabadkai, G.; Duchen, M. R.; Campbell, M.; Cuenca, S. R.; Vidal-Puig, A.; James, A. M.; Murphy, M. P.; Filonenko, V.; Skehel, M.; Gout, I. Protein CoAlation: A Redox-Regulated Protein Modification by Coenzyme A in Mammalian Cells. *Biochem. J.* **2017**, *474* (14), 2489–2508. https://doi.org/10.1042/BCJ20170129.
(16) Filonenko, V.; Gout, I. Discovery and Functional Characterisation of Protein CoAlation and the Antioxidant Function of Coenzyme A. *BBA Adv.* **2023**, *3*, 100075. https://doi.org/10.1016/j.bbadva.2023.100075.
(17) Yu, Y.; Moretti, I. F.; Grzeschik, N. A.; Sibon, O. C. M.; Schepers, H. Coenzyme A Levels Influence Protein Acetylation, CoAlation and 4′-Phosphopantetheinylation: Expanding the Impact of a Metabolic Nexus Molecule. *Biochim. Biophys. Acta BBA - Mol. Cell Res.* **2021**, *1868* (4), 118965. https://doi.org/10.1016/j.bbamcr.2021.118965.
(18) Gout, I. Coenzyme A, Protein CoAlation and Redox Regulation in Mammalian Cells. *Biochem. Soc. Trans.* **2018**, *46* (3), 721–728. https://doi.org/10.1042/BST20170506.
(19) Naquet, P.; Kerr, E. W.; Vickers, S. D.; Leonardi, R. Regulation of Coenzyme A Levels by Degradation: The 'Ins and Outs.' *Prog. Lipid Res.* **2020**, *78*, 101028. https://doi.org/10.1016/j.plipres.2020.101028.
(20) Fiermonte, G.; Paradies, E.; Todisco, S.; Marobbio, C. M. T.; Palmieri, F. A Novel Member of Solute Carrier Family 25 (SLC25A42) Is a Transporter of Coenzyme A and Adenosine 3′,5′-Diphosphate in Human Mitochondria *. *J. Biol. Chem.* **2009**, *284* (27), 18152–18159. https://doi.org/10.1074/jbc.M109.014118.
(21) Sugiura, Y.; Tanaka, H.; Kuroda, Y. Selection of Binding Sites in Coenzyme A by Nickel(II) and Copper(II). *Chem. Lett.* **1976**, *5* (3), 193–198. https://doi.org/10.1246/cl.1976.193.
(22) Zea, C. J.; Camci-Unal, G.; Pohl, N. L. Thermodynamics of Binding of Divalent Magnesium and Manganese to Uridine Phosphates: Implications for Diabetes-Related Hypomagnesaemia and Carbohydrate Biocatalysis. *Chem. Cent. J.* **2008**, *2* (1), 15. https://doi.org/10.1186/1752-153X-2-15.
(23) Andries, C.; Manea, M.; Drochioiu, G.; Gradinaru, R. New Insights into Coenzyme A Interaction with Mercury Ions Provided by Mass Spectrometric and Circular Dichroism Spectroscopic Approaches. *Eur. J. Mass Spectrom.* **2015**, *21* (2), 97–102. https://doi.org/10.1255/ejms.1361.
(24) Wilson, G. E. Magnetic Resonance Studies of the Conformation of Manganese (II) Coenzyme A. *FEBS Lett.* **1979**, *105* (1), 81–84. https://doi.org/10.1016/0014-5793(79)80891-1.
(25) Storer, A. C.; Cornish-Bowden, A. Concentration of MgATP2- and Other Ions in Solution. Calculation of the True Concentrations of Species Present in Mixtures of Associating Ions. *Biochem. J.* **1976**, *159* (1), 1–5. https://doi.org/10.1042/bj1590001.
(26) Wilson, J. E.; Chin, A. Chelation of Divalent Cations by ATP, Studied by Titration Calorimetry. *Anal. Biochem.* **1991**, *193* (1), 16–19. https://doi.org/10.1016/0003-2697(91)90036-S.
(27) Walker, B.; Jing, Z.; Ren, P. Molecular Dynamics Free Energy Simulations of ATP:Mg2+ and ADP:Mg2+ Using the Polarisable Force Field AMOEBA. *Mol. Simul.* **2021**, *47* (5), 439–448. https://doi.org/10.1080/08927022.2020.1725003.
(28) Gallo, A. A.; Hansen, I. L.; Sable, H. Z.; Swift, T. J. Coenzyme Interactions. *J. Biol. Chem.* **1972**, *247* (18), 5913–5920. https://doi.org/10.1016/S0021-9258(19)44845-X.
(29) Lee, L. P. K.; Kosicki, G. W. Effect Of Magnesium Ions On Coenzyme A And Pyrophosphate Derivatives Inhibition Of Yeast Glucose-6-Phosphate Dehydrogenase. *Can. J. Biochem.* **1967**, *45* (8), 1279–1282. https://doi.org/10.1139/o67-149.

(30) Tossounian, M.-A.; Baczynska, M.; Dalton, W.; Newell, C.; Ma, Y.; Das, S.; Semelak, J. A.; Estrin, D. A.; Filonenko, V.; Trujillo, M.; Peak-Chew, S. Y.; Skehel, M.; Fraternali, F.; Orengo, C.; Gout, I. Profiling the Site of Protein CoAlation and Coenzyme A Stabilization Interactions. *Antioxidants* **2022**, *11* (7), 1362. https://doi.org/10.3390/antiox11071362.

(31) Jung, J.; Bashiri, G.; Johnston, J. M.; Brown, A. S.; Ackerley, D. F.; Baker, E. N. Crystal Structure of the Essential Mycobacterium Tuberculosis Phosphopantetheinyl Transferase PptT, Solved as a Fusion Protein with Maltose Binding Protein. *J. Struct. Biol.* **2014**, *188* (3), 274–278. https://doi.org/10.1016/j.jsb.2014.10.004.

(32) Giljanović, J.; Prkić, A. Determination of Coenzyme A (CoASH) in the Presence of Different Thiols by Using Flow-Injection with a UV/Vis Spectrophotometric Detector and Potentiometric Determination of CoASH Using an Iodide ISE. *Molecules* **2010**, *15* (1), 100–113. https://doi.org/10.3390/molecules15010100.

(33) Riddles, P. W.; Blakeley, R. L.; Zerner, B. [8] Reassessment of Ellman's Reagent. In *Methods in Enzymology*; Enzyme Structure Part I; Academic Press, 1983; Vol. 91, pp 49–60. https://doi.org/10.1016/S0076-6879(83)91010-8.

(34) delCardayré, S. B.; Stock, K. P.; Newton, G. L.; Fahey, R. C.; Davies, J. E. Coenzyme A Disulfide Reductase, the Primary Low Molecular Weight Disulfide Reductase from Staphylococcus Aureus: PURIFICATION AND CHARACTERIZATION OF THE NATIVE ENZYME *. *J. Biol. Chem.* **1998**, *273* (10), 5744–5751. https://doi.org/10.1074/jbc.273.10.5744.

(35) Velazquez-Campoy, A.; Claro, B.; Abian, O.; Höring, J.; Bourlon, L.; Claveria-Gimeno, R.; Ennifar, E.; England, P.; Chaires, J. B.; Wu, D.; Piszczek, G.; Brautigam, C.; Tso, S.-C.; Zhao, H.; Schuck, P.; Keller, S.; Bastos, M. A Multi-Laboratory Benchmark Study of Isothermal Titration Calorimetry (ITC) Using Ca2+ and Mg2+ Binding to EDTA. *Eur. Biophys. J.* **2021**, *50* (3–4), 429–451. https://doi.org/10.1007/s00249-021-01523-7.

(36) Kemmer, G.; Keller, S. Nonlinear Least-Squares Data Fitting in Excel Spreadsheets. *Nat. Protoc.* **2010**, *5* (2), 267–281. https://doi.org/10.1038/nprot.2009.182.

(37) Cattoni, D. I.; Kaufman, S. B.; González Flecha, F. L. Kinetics and Thermodynamics of the Interaction of 1-Anilino-Naphthalene-8-Sulfonate with Proteins. *Biochim. Biophys. Acta BBA - Proteins Proteomics* **2009**, *1794* (11), 1700–1708. https://doi.org/10.1016/j.bbapap.2009.08.007.

(38) Williamson, M. P. Using Chemical Shift Perturbation to Characterise Ligand Binding. *Prog. Nucl. Magn. Reson. Spectrosc.* **2013**, *73*, 1–16. https://doi.org/10.1016/j.pnmrs.2013.02.001.

(39) Schleucher, J.; Schwendinger, M.; Sattler, M.; Schmidt, P.; Schedletzky, O.; Glaser, S. J.; Sørensen, O. W.; Griesinger, C. A General Enhancement Scheme in Heteronuclear Multidimensional NMR Employing Pulsed Field Gradients. *J. Biomol. NMR* **1994**, *4* (2), 301–306. https://doi.org/10.1007/BF00175254.

(40) Dordine, R. L.; Paneth, P.; Anderson, V. E. 13C NMR and 1H-1H NOEs of Coenzyme-A: Conformation of the Pantoic Acid Moiety. *Bioorganic Chem.* **1995**, *23* (2), 169–181. https://doi.org/10.1006/bioo.1995.1014.

(41) D.A. Case, R.M. Betz, D.S. Cerutti, T.E. Cheatham, III, T.A. Darden, R.E. Duke, T.J. Giese, H. Gohlke,; A.W. Goetz, N. Homeyer, S. Izadi, P. Janowski, J. Kaus, A. Kovalenko, T.S. Lee, S. LeGrand, P. Li, C.; Lin, T. Luchko, R. Luo, B. Madej, D. Mermelstein, K.M. Merz, G. Monard, H. Nguyen, H.T. Nguyen, I.; Omelyan, A. Onufriev, D.R. Roe, A. Roitberg, C. Sagui, C.L. Simmerling, W.M. Botello-Smith, J. Swails,; R.C. Walker, J. Wang, R.M. Wolf, X. Wu, L. Xiao and P.A. Kollman. Amber 16.

(42) Wang, J.; Wolf, R. M.; Caldwell, J. W.; Kollman, P. A.; Case, D. A. Development and Testing of a General Amber Force Field. *J. Comput. Chem.* **2004**, *25* (9), 1157–1174. https://doi.org/10.1002/jcc.20035.

(43) Bayly, C. I.; Cieplak, P.; Cornell, W.; Kollman, P. A. A Well-Behaved Electrostatic Potential Based Method Using Charge Restraints for Deriving Atomic Charges: The RESP Model. *J. Phys. Chem.* **1993**, *97* (40), 10269–10280. https://doi.org/10.1021/j100142a004.

(44) Frisch, M. J.; Trucks, G. W.; Cheeseman, J. R.; Scalmani, G.; Caricato, M.; Hratchian, H. P.; Li, X.; Barone, V.; Bloino, J.; Zheng, G.; Vreven, T.; Montgomery, J. A.; Petersson, G. A.; Scuseria, G. E.; Schlegel, H. B.; Nakatsuji, H.; Izmaylov, A. F.; Martin, R. L.; Sonnenberg, J. L.; Peralta, J. E.; Heyd, J. J.; Brothers, E.; Ogliaro,

F.; Bearpark, M.; Robb, M. A.; Mennucci, B.; Kudin, K. N.; Staroverov, V. N.; Kobayashi, R.; Normand, J.; Rendell, A.; Gomperts, R.; Zakrzewski, V. G.; Hada, M.; Ehara, M.; Toyota, K.; Fukuda, R.; Hasegawa, J.; Ishida, M.; Nakajima, T.; Honda, Y.; Kitao, O.; Nakai, H. Gaussian 09.

(45) Åqvist, J. Ion-Water Interaction Potentials Derived from Free Energy Perturbation Simulations. *J. Phys. Chem.* **1990**, *94* (21), 8021–8024. https://doi.org/10.1021/j100384a009.

(46) Smith, D. E.; Dang, L. X. Computer Simulations of NaCl Association in Polarizable Water. *J. Chem. Phys.* **1994**, *100* (5), 3757–3766. https://doi.org/10.1063/1.466363.

(47) Kräutler, V.; van Gunsteren, W. F.; Hünenberger, P. H. A Fast SHAKE Algorithm to Solve Distance Constraint Equations for Small Molecules in Molecular Dynamics Simulations. *J. Comput. Chem.* **2001**, *22* (5), 501–508. https://doi.org/10.1002/1096-987X(20010415)22:5<501::AID-JCC1021>3.0.CO;2-V.

(48) Berendsen, H. J. C.; Postma, J. P. M.; van Gunsteren, W. F.; DiNola, A.; Haak, J. R. Molecular Dynamics with Coupling to an External Bath. *J. Chem. Phys.* **1984**, *81* (8), 3684–3690. https://doi.org/10.1063/1.448118.

(49) Davidchack, R. L.; Handel, R.; Tretyakov, M. V. Langevin Thermostat for Rigid Body Dynamics. *J. Chem. Phys.* **2009**, *130* (23), 234101. https://doi.org/10.1063/1.3149788.

(50) Schlitter, J. Estimation of Absolute and Relative Entropies of Macromolecules Using the Covariance Matrix. *Chem. Phys. Lett.* **1993**, *215* (6), 617–621. https://doi.org/10.1016/0009-2614(93)89366-P.

(51) Schäfer, H.; Mark, A. E.; van Gunsteren, W. F. Absolute Entropies from Molecular Dynamics Simulation Trajectories. *J. Chem. Phys.* **2000**, *113* (18), 7809–7817. https://doi.org/10.1063/1.1309534.

(52) Schäfer, H.; Daura, X.; Mark, A. E.; van Gunsteren, W. F. Entropy Calculations on a Reversibly Folding Peptide: Changes in Solute Free Energy Cannot Explain Folding Behavior. *Proteins Struct. Funct. Bioinforma.* **2001**, *43* (1), 45–56. https://doi.org/10.1002/1097-0134(20010401)43:1<45::AID-PROT1016>3.0.CO;2-N.

(53) Harris, S. A.; Gavathiotis, E.; Searle, M. S.; Orozco, M.; Laughton, C. A. Cooperativity in Drug−DNA Recognition: A Molecular Dynamics Study. *J. Am. Chem. Soc.* **2001**, *123* (50), 12658–12663. https://doi.org/10.1021/ja016233n.

(54) Harris, S. A.; Sands, Z. A.; Laughton, C. A. Molecular Dynamics Simulations of Duplex Stretching Reveal the Importance of Entropy in Determining the Biomechanical Properties of DNA. *Biophys. J.* **2005**, *88* (3), 1684–1691. https://doi.org/10.1529/biophysj.104.046912.

(55) Roe, D. R.; Cheatham, T. E. I. PTRAJ and CPPTRAJ: Software for Processing and Analysis of Molecular Dynamics Trajectory Data. *J. Chem. Theory Comput.* **2013**, *9* (7), 3084–3095. https://doi.org/10.1021/ct400341p.

(56) Glielmo, A.; Macocco, I.; Doimo, D.; Carli, M.; Zeni, C.; Wild, R.; d'Errico, M.; Rodriguez, A.; Laio, A. DADApy: Distance-Based Analysis of Data-Manifolds in Python. *Patterns* **2022**, *3* (10), 100589. https://doi.org/10.1016/j.patter.2022.100589.

(57) Rodriguez, A.; Laio, A. Clustering by Fast Search and Find of Density Peaks. *Science* **2014**, *344* (6191), 1492–1496. https://doi.org/10.1126/science.1242072.

(58) Campadelli, P.; Casiraghi, E.; Ceruti, C.; Rozza, A. Intrinsic Dimension Estimation: Relevant Techniques and a Benchmark Framework. *Math. Probl. Eng.* **2015**, *2015*, e759567. https://doi.org/10.1155/2015/759567.

(59) Facco, E.; d'Errico, M.; Rodriguez, A.; Laio, A. Estimating the Intrinsic Dimension of Datasets by a Minimal Neighborhood Information. *Sci. Rep.* **2017**, *7* (1), 12140. https://doi.org/10.1038/s41598-017-11873-y.

(60) Rew, R.; Davis, G. NetCDF: An Interface for Scientific Data Access. *IEEE Comput. Graph. Appl.* **1990**, *10* (4), 76–82. https://doi.org/10.1109/38.56302.

(61) Shirts, M. R.; Klein, C.; Swails, J. M.; Yin, J.; Gilson, M. K.; Mobley, D. L.; Case, D. A.; Zhong, E. D. Lessons Learned from Comparing Molecular Dynamics Engines on the SAMPL5 Dataset. *J. Comput. Aided Mol. Des.* **2017**, *31* (1), 147–161. https://doi.org/10.1007/s10822-016-9977-1.

(62) McInnes, L.; Healy, J.; Melville, J. UMAP: Uniform Manifold Approximation and Projection for Dimension Reduction. arXiv September 17, 2020. https://doi.org/10.48550/arXiv.1802.03426.

(63) Llopis, J.; McCaffery, J. M.; Miyawaki, A.; Farquhar, M. G.; Tsien, R. Y. Measurement of Cytosolic,

Mitochondrial, and Golgi pH in Single Living Cells with Green Fluorescent Proteins. *Proc. Natl. Acad. Sci.* **1998**, *95* (12), 6803–6808. https://doi.org/10.1073/pnas.95.12.6803.

(64) Kumar, G. D.; Banasiewicz, M.; Wrzosek, A.; Kampa, R. P.; Bousquet, M. H. E.; Kusy, D.; Jacquemin, D.; Szewczyk, A.; Gryko, D. T. Probing the Flux of Mitochondrial Potassium Using an Azacrown-Diketopyrrolopyrrole Based Highly Sensitive Probe. *Chem. Commun.* **2022**, *58* (28), 4500–4503. https://doi.org/10.1039/D2CC00324D.

(65) Terzioglu, M.; Veeroja, K.; Montonen, T.; Ihalainen, T. O.; Salminen, T. S.; Bénit, P.; Rustin, P.; Chang, Y.-T.; Nagai, T.; Jacobs, H. T. Mitochondrial Temperature Homeostasis Resists External Metabolic Stresses. *eLife* **2023**, *12*, RP89232. https://doi.org/10.7554/eLife.89232.3.

(66) Corkey, B. E.; Duszynski, J.; Rich, T. L.; Matschinsky, B.; Williamson, J. R. Regulation of Free and Bound Magnesium in Rat Hepatocytes and Isolated Mitochondria. *J. Biol. Chem.* **1986**, *261* (6), 2567–2574. https://doi.org/10.1016/S0021-9258(17)35825-8.

(67) Jung, D. W.; Brierley, G. P. Magnesium Transport by Mitochondria. *J. Bioenerg. Biomembr.* **1994**, *26* (5), 527–535. https://doi.org/10.1007/BF00762737.

(68) Rutter, G. A.; Osbaldeston, N. J.; McCormack, J. G.; Denton, R. M. Measurement of Matrix Free Mg2+ Concentration in Rat Heart Mitochondria by Using Entrapped Fluorescent Probes. *Biochem. J.* **1990**, *271* (3), 627–634. https://doi.org/10.1042/bj2710627.

(69) Lane, N. Hot Mitochondria? *PLoS Biol.* **2018**, *16* (1), e2005113. https://doi.org/10.1371/journal.pbio.2005113.

(70) Macherel, D.; Haraux, F.; Guillou, H.; Bourgeois, O. The Conundrum of Hot Mitochondria. *Biochim. Biophys. Acta BBA - Bioenerg.* **2021**, *1862* (2), 148348. https://doi.org/10.1016/j.bbabio.2020.148348.

(71) El-Gammal, Z.; Nasr, M. A.; Elmehrath, A. O.; Salah, R. A.; Saad, S. M.; El-Badri, N. Regulation of Mitochondrial Temperature in Health and Disease. *Pflüg. Arch. - Eur. J. Physiol.* **2022**, *474* (10), 1043–1051. https://doi.org/10.1007/s00424-022-02719-2.

(72) Nagana Gowda, G. A.; Abell, L.; Tian, R. Extending the Scope of 1H NMR Spectroscopy for the Analysis of Cellular Coenzyme A and Acetyl Coenzyme A. *Anal. Chem.* **2019**, *91* (3), 2464–2471. https://doi.org/10.1021/acs.analchem.8b05286.

(73) McEwen, I. Broadening of 1H NMR Signals in the Spectra of Heparin and OSCS by Paramagnetic Transition Metal Ions. The Use of EDTA to Sharpen the Signals. *J. Pharm. Biomed. Anal.* **2010**, *51* (3), 733–735. https://doi.org/10.1016/j.jpba.2009.09.009.

(74) Christensen, M.; Jacobsen, J. P. 31P NMR Relaxation Time Studies of 2,3-Diphosphoglycerate in Solution and Intact Erythrocytes. *Magn. Reson. Med.* **1988**, *7* (2), 197–203. https://doi.org/10.1002/mrm.1910070207.

(75) Frick, D. N.; Weber, D. J.; Abeygunawardana, C.; Gittis, A. G.; Bessman, M. J.; Mildvan, A. S. NMR Studies of the Conformations and Location of Nucleotides Bound to the Escherichia Coli MutT Enzyme. *Biochemistry* **1995**, *34* (16), 5577–5586. https://doi.org/10.1021/bi00016a032.

(76) Hove-Jensen, B.; McSorley, F. R.; Zechel, D. L. Catabolism and Detoxification of 1-Aminoalkylphosphonic Acids: N-Acetylation by the phnO Gene Product. *PLOS ONE* **2012**, *7* (10), e46416. https://doi.org/10.1371/journal.pone.0046416.

(77) McCoy, F.; Darbandi, R.; Lee, H. C.; Bharatham, K.; Moldoveanu, T.; Grace, C. R.; Dodd, K.; Lin, W.; Chen, S.-I.; Tangallapally, R. P.; Kurokawa, M.; Lee, R. E.; Shelat, A. A.; Chen, T.; Green, D. R.; Harris, R. A.; Lin, S.-H.; Fissore, R. A.; Colbran, R. J.; Nutt, L. K. Metabolic Activation of CaMKII by Coenzyme A. *Mol. Cell* **2013**, *52* (3), 325–339. https://doi.org/10.1016/j.molcel.2013.08.043.

(78) Shi, S.; Lin, J.; Cai, Y.; Yu, J.; Hong, H.; Ji, K.; Downey, J. S.; Lu, X.; Chen, R.; Han, J.; Han, A. Dimeric Structure of P300/CBP Associated Factor. *BMC Struct. Biol.* **2014**, *14* (1), 2. https://doi.org/10.1186/1472-6807-14-2.

(79) Peterson, K. L.; Srivastava, D. K. Functional Role of a Distal (3′-Phosphate) Group of CoA in the Recombinant Human Liver Medium-Chain Acyl-CoA Dehydrogenase-Catalysed Reaction. *Biochem. J.* **1997**, *325* (3), 751–760. https://doi.org/10.1042/bj3250751.

(80) Scorpio, R. M.; Masoro, E. J. Differences between Manganese and Magnesium Ions with Regard to Fatty Acid Biosynthesis, Acetyl-Coenzyme A Carboxylase Activity and Malonyl-Coenzyme A Decarboxylation. *Biochem. J.* **1970**, *118* (3), 391–399. https://doi.org/10.1042/bj1180391.
(81) Li, L. O.; Klett, E. L.; Coleman, R. A. Acyl-CoA Synthesis, Lipid Metabolism and Lipotoxicity. *Biochim. Biophys. Acta BBA - Mol. Cell Biol. Lipids* **2010**, *1801* (3), 246–251. https://doi.org/10.1016/j.bbalip.2009.09.024.
(82) Buttlaire, D. H.; Chon, M. Interactions of Phospho- and Dephosphosuccinyl Coenzyme A Synthetase with Manganous Ion and Substrates. Studies of Manganese Complexes by NMR Relaxation Rates of Water Protons. *J. Biol. Chem.* **1977**, *252* (6), 1957–1964. https://doi.org/10.1016/S0021-9258(18)71850-4.
(83) Laliberté, J. F.; St-Jean, P.; Beaudoin, A. R. Kinetic Effects of Ca2+ and Mg2+ on ATP Hydrolysis by the Purified ATP Diphosphohydrolase. *J. Biol. Chem.* **1982**, *257* (7), 3869–3874. https://doi.org/10.1016/S0021-9258(18)34863-4.
(84) Yeh, L. A.; Song, C. S.; Kim, K. H. Coenzyme A Activation of Acetyl-CoA Carboxylase. *J. Biol. Chem.* **1981**, *256* (5), 2289–2296. https://doi.org/10.1016/S0021-9258(19)69776-0.
(85) Tsuchiya, Y.; Byrne, D. P.; Burgess, S. G.; Bormann, J.; Baković, J.; Huang, Y.; Zhyvoloup, A.; Yu, B. Y. K.; Peak-Chew, S.; Tran, T.; Bellany, F.; Tabor, A. B.; Chan, A. E.; Guruprasad, L.; Garifulin, O.; Filonenko, V.; Vonderach, M.; Ferries, S.; Eyers, C. E.; Carroll, J.; Skehel, M.; Bayliss, R.; Eyers, P. A.; Gout, I. Covalent Aurora A Regulation by the Metabolic Integrator Coenzyme A. *Redox Biol.* **2020**, *28*, 101318. https://doi.org/10.1016/j.redox.2019.101318.